

Temperature-dependent “phason” elasticity in a random tiling quasicrystal

M. Mihalkovič* and C. L. Henley

Dept. of Physics, Cornell University, Ithaca NY 14853-2501

Both “phason” elastic constants have been measured from Monte Carlo simulations of a random-tiling icosahedral quasicrystal model with a Hamiltonian. The low-temperature limit approximates the “canonical-cell” tiling used to describe several real quasicrystals. The elastic constant K_2 changes sign from positive to negative with decreasing temperature; in the “canonical-cell” limit, K_2/K_1 appears to approach -0.7 , about the critical value for a phason-mode modulation instability. We compare to the experiments on i -AlPdMn and i -AlCuFe.

PACS numbers: 61.44.Br, 62.20.Dc, 5.10.Ln, 64.60.Cn

Quasicrystals possess translational long-range order, as manifested by resolution-limited Bragg peaks¹, yet possess symmetries (e.g. icosahedral) incompatible with periodicity. The best-understood quasicrystals can be represented as rigid tilings (or cluster networks) decorated by atoms in a uniform fashion^{2,3,4,5}. Their long-range order can then be investigated in a purely tiling framework, being determined by the “tile Hamiltonian”^{2,5}), which assigns to every tiling the corresponding structural energy.

Despite years of study, there remain two plausible, competing scenarios that predict quasicrystal long-range order (in the sense that *both* predict Bragg peaks in dimension $d > 2$.) The “ideal tiling” scenario postulates that the tile Hamiltonian enforces an essentially unique, perfectly quasiperiodic ground state analogous to a perfect crystal (just as matching rules or covering rules^{6,7} enforce a Penrose tiling). Alternatively, the (equilibrium) “random tiling” scenario supposes an ensemble of many *nearly* degenerate packings of the structural units. Then the true ground state is normally a coexistence of crystal phases, but at higher temperatures the random-tiling quasicrystal becomes thermodynamically stable owing to its larger entropy (See references cited in 2).

The two scenarios may be distinguished experimentally by their diffuse scattering. In the random-tiling case, every Bragg peak is surrounded by wings of diffuse scattering with distinctive shapes predicted by the “phason” elastic theory⁸. (See (8), below.) Those shapes were observed in X-ray and neutron diffraction of i -AlPdMn^{9,10} and i -AlCuFe¹¹, and the fitted phason-elastic constants were temperature-dependent.

In this Letter, we simulate random tilings of rhombohedra with a tile Hamiltonian that favors configurations approximating a “canonical cell tiling”^{3,12} (CCT). Our motives are (1) to infer the phason elastic constants of the CCT, which is difficult to simulate directly, and (2) to observe the crossover with decreasing temperature T as clusters of small (rhombohedral) tiles get bound together into larger (CCT) “supertiles” in a toy model. The same techniques will be essential in computing the phason elastic constants for models of specific real quasicrystals.

I. CANONICAL-CELL TILING AND HAMILTONIAN

Atomic structure models of i -AlZnMg⁴ [or i -AlMnSi⁵], and many related alloys, may be built by placing icosahedral “Bergman” [or “MI”] clusters on the nodes of networks with inter-node linkages of two lengths: $b \equiv 2.75a_R$ along twofold symmetry directions or $c \equiv 2.38a_R$ along threefold directions, which we shall call a “ bc -network.” (The quasilattice constant a_R is set to unity in this paper; $a_R \approx 0.5\text{nm}$ in real quasicrystals.) A “canonical-cell” tiling³ (CCT) is a special bc -network built from the four smallest polyhedral cells having b or c edges.

A Monte Carlo simulation of the CCT is practically intractable, since *local* tile reshufflings do not exist: spatially extended clusters must be rearranged to reach another valid tiling^{3,13}. To circumvent this problem, our model system is a bc network in which the CCT constraints are not imposed, but are favored by a Hamiltonian and thus satisfied in the limit $T \rightarrow 0$. We emphasize that unlike matching-rule Hamiltonians,¹⁴ eq. (1) does *not* force a unique quasiperiodic $T = 0$ state; the ground state ensemble is still a random tiling, but a different one (with less entropy) than at $T = \infty$. Our configuration space is the random “three-dimensional Penrose tiling” (3DPT), which includes all packings of the well-known oblate and prolate rhombohedra having edges of length $a_R \equiv 1$ along 5-fold symmetry directions. Similar simulations of another imperfect approximation of the CCT by a bc -network, namely the lattice-gas of Ref. 12, will be reported elsewhere.¹⁵

The 3DPT contains a special subset of vertices, called “12-fold” nodes, at which rhombohedron edges emanate in all 12 of the five-fold symmetry directions¹⁶. This 12-fold network approximates the CCT, since the separation of nearby nodes is usually a b or c linkage; however a “short” separation of a_R (along 5-fold axes) occurs rarely. For our simulations, we adopted the Hamiltonian

$$\mathcal{H}_{12} = -N_{12} + \alpha_{\text{short}} N_{sb}, \quad (1)$$

where N_{12} is the total number of 12-fold nodes, and N_{sb} is the number of “short” node pairs with separation a_R .

The purpose of α_{short} is to suppress “short” pairs; $\alpha_{\text{short}} \equiv 1$ suffices, which we adopted after testing other

values. We conjecture (and simulations support) that the ground states of (1) are a subset of CCT's, namely those with maximum node density, and not the maximum-entropy random CCT.

II. PERPENDICULAR SPACE AND FLUCTUATIONS

Our rhombohedron edges are $\pm \mathbf{e}^\parallel_\alpha$, where¹⁷ $\mathbf{e}^\parallel_1 = (\tau, 0, 1)/(1 + \tau^2)^{1/2}$ and the other basis vectors are made by reflections in the x , y , or z planes, or by cyclic permutation of the components. Thus every vertex has coordinates of the form

$$\mathbf{x}^\parallel = \sum_{\alpha=1}^6 n_\alpha \mathbf{e}^\parallel_\alpha, \quad (2)$$

In a standard trick, the integer coefficients may be visualized as coordinates $\mathbf{x} = [n_1, \dots, n_6]$ of a 6-dimensional hypercubic lattice, into which eq. (2) embeds a 3-surface¹⁸. This 3-surface is conveniently parametrized by a “perpendicular” (“perp”) coordinate, defined for each vertex by

$$\mathbf{x}^\perp = \sum_{\alpha=1}^6 n_\alpha \mathbf{e}^\perp_\alpha, \quad (3)$$

where $\mathbf{e}^\perp_1 = \eta(1, 0, -\tau)/(1 + \tau^2)^{1/2}$ and the other basis vectors \mathbf{e}^\perp_α are derived by the same reflections and cyclic permutations used to produce $\mathbf{e}^\parallel_\alpha$ from \mathbf{e}^\parallel_1 . We write $\mathbf{h}(\mathbf{r})$ for the smoothed (coarse-grained) version of \mathbf{x}^\perp .

The gradients $\nabla \mathbf{h}(\mathbf{r})$, forming the “phason strain” tensor, quantify the local deviation from icosahedral symmetry. The random-tiling scenario² predicts that a quasicrystal’s free energy density has a *phason elastic* form,¹⁹ i.e. is quadratic in components of $\nabla \mathbf{h}$. This was confirmed numerically for several completely random ($T = \infty$) tilings^{3,13,20,21,22}, but not until now for the CCT. In contrast, the “ideal tiling” behavior implies a free energy scaling as $|\nabla \mathbf{h}|$. An icosahedral quasicrystal has two elastic constants, K_1 and K_2 . Very roughly speaking, K_1 parametrizes the mean strength of the elastic stiffness, and K_2 parametrizes its anisotropy (degree of coupling between direction of the gradient in real space and components of \mathbf{h}).

For fluctuations around a state with zero mean phason strain, the dimensionless elastic free energy is^{17,19}

$$F/T = \frac{1}{2} \sum_{\mathbf{q}, ij} C_{ij}(\mathbf{q}) \tilde{h}_i(\mathbf{q}) \tilde{h}_j(-\mathbf{q}) \quad (4)$$

where it is convenient to use $\tilde{\mathbf{h}}(\mathbf{q}) \equiv V^{-1/2} \int d^3 \mathbf{r} e^{-i\mathbf{q} \cdot \mathbf{r}} \mathbf{h}(\mathbf{r})$. Here

$$C_{ij}(\mathbf{q}) = K_1 |\mathbf{q}|^2 \delta_{ij} - K_2 \left[\left(\frac{1}{3} |\mathbf{q}|^2 + 2q_i^2 + q_{i+1}^2/\tau - \tau q_{i-1}^2 \right) \delta_{ij} - 2q_i q_j \right]. \quad (5)$$

Eq. (4) implies that each $\tilde{\mathbf{h}}(\mathbf{q})$ consists of Gaussian random variables, and their correlations

$$\Gamma_{ij}(\mathbf{q}) \equiv \langle \tilde{h}_i(-\mathbf{q}) \tilde{h}_j(\mathbf{q}) \rangle. \quad (6)$$

are given by

$$\Gamma_{ij}(\mathbf{q}) = [C(\mathbf{q})^{-1}]_{ij}. \quad (7)$$

The diffuse diffraction intensity⁸ near a Bragg peak with reciprocal lattice vector \mathbf{G}^\parallel is

$$I(\mathbf{q}) \propto \sum_{ij} G_i^\perp \Gamma_{ij}(\mathbf{q}) G_j^\perp, \quad (8)$$

where \mathbf{G}^\perp is the perp-space partner of \mathbf{G}^\parallel . (An equilibrium random tiling in $d > 2$ has true Bragg peaks^{2,18} as well as diffuse scattering.) Experiments measure (8); simulations can measure (6) directly.

III. SIMULATION, MEASUREMENTS, AND CORRECTIONS

Our data is taken from tilings using periodic boundary conditions in a cubic cell of side $L = \tau^6(2 - 2/\sqrt{5})^{1/2} a_R = 18.868 a_R$. This corresponds to the “8/5 Fibonacci approximant” of the 3DPT²², and contains $N_v = 10336$ rhombohedron vertices. We use the very simple update move for the 3DPT which rearranges the four tiles surrounding a vertex with just four edges.^{21,22}

Simulation time is measured in Monte Carlo sweeps, where each sweep makes N_v actual flips on randomly chosen vertices. A simulation run consisted of 500 thermal cycles; each cycle included 3000 MCS at $T = \infty$ (to erase memory of the preceding cycle), followed by 34 cooling stages each at a constant temperature. Each stage takes 1000 MCS, except the first six stages ($T > 0.8$) used 200 to 800 MCS; 10 measurements were made during the last 100 MCS of each stage. A typical 8/5 cooling run took 10 days of CPU time on a 1.5 GHz Athlon processor.

We constructed \mathbf{x}^\parallel and \mathbf{x}^\perp for each vertex, using (2) and (3). For each \mathbf{q} on a standard list of 70 wavevectors, we took

$$\tilde{\mathbf{H}}(\mathbf{q}) \equiv \frac{\sqrt{V}}{N_v} \sum_{\mathbf{x} \in 3\text{DPT}} \mathbf{x}^\perp e^{-i\mathbf{q} \cdot \mathbf{x}^\parallel} \quad (9)$$

as in Ref. 22, where V is the simulation cell volume and the sum runs over the N_v actual 3DPT vertices. The normalization in (9) ensures that $\tilde{\mathbf{H}}(\mathbf{q}) \approx \tilde{\mathbf{h}}(\mathbf{q})$ for small \mathbf{q} . Fluctuation correlations analogous to (6), $\Gamma_{ij}^H(\mathbf{q}) \equiv \langle \tilde{\mathbf{H}}_i(-\mathbf{q}) \tilde{\mathbf{H}}_j(\mathbf{q}) \rangle$ were accumulated, and were symmetrized with respect to cyclic permutations (xyz).

Although $\langle \tilde{\mathbf{h}}(\mathbf{q}) \rangle = 0$, Eq. (9) has a nonzero expectation when \mathbf{q} is a Bragg vector, just like the structure factor, from which the sum (9) differs only by the extra factor \mathbf{x}^\perp . As in the structure factor, each Bragg peak of our $\Gamma^H(\mathbf{q})$ function is surrounded by a tail of diffuse scattering, which must also be subtracted in order to correct

the nearby wavevectors. To calculate this tail, we adopt the “undulating cut approximation” (Ref. 2, Sec. 7), in which the occupation probability of a physical-space vertex \mathbf{x}^\parallel is $\rho_0(\mathbf{x}^\perp - \mathbf{h}(\mathbf{x}^\parallel)) \leq 1$. Here \mathbf{x}^\parallel and \mathbf{x}^\perp are related as in eqs. (2) and (3), $\mathbf{h}(\mathbf{r})$ is smooth and fluctuating according to (7), and $\rho_0(\mathbf{h})$ defines an ideal reference structure when \mathbf{h} is flat. The measured fluctuation is predicted to be¹⁵

$$\Gamma_{ij}^H(\mathbf{q}) = \Gamma_{ij}(\mathbf{q}) + \sum_{\mathbf{G}^\parallel} \Gamma_{ij}^{\text{Bragg}}(\mathbf{q}, \mathbf{G}^\parallel). \quad (10)$$

where

$$\Gamma_{ij}^{\text{Bragg}}(\mathbf{q}; \mathbf{G}^\parallel) = D_i D_j \left[V \delta_{\mathbf{q}, \mathbf{G}^\perp} + (\mathbf{G}^\perp, \Gamma(\mathbf{q} - \mathbf{G}^\parallel) \mathbf{G}^\perp) \right]. \quad (11)$$

Here $\mathbf{D} = \mathbf{D}(\mathbf{G}^\perp)$ can be expressed¹⁵ in terms of the Fourier transform of $\rho_0(\mathbf{x}^\perp)$; in light of the symmetry, $\mathbf{D}(\mathbf{G}^\perp) \parallel \mathbf{G}^\perp$ along any symmetry axis.

Our measurements include one orbit of weak Bragg peaks on 3-fold symmetry axes, – at $\mathbf{G}^\parallel = \frac{2\pi}{L}(333)$ and $\frac{2\pi}{L}(520)$ in our cell – where the Bragg intensity contributes far stronger than the long-wavelength fluctuations (6). We determined each Bragg term (first term in (11), i.e. $D_i D_m$) from $\langle \tilde{\mathbf{h}}(\mathbf{q}) \rangle$ averaged over each temperature stage²³. From our estimate of K_1 and K_2 , we know $\Gamma(\mathbf{q})$ via (7), hence the second term in (11), so we can subtract the sum in (10) from the measured data. The resulting matrices $\Gamma(\mathbf{q})$ are inverted to obtain (via (7)) estimates of (5), which are fitted to K_1 and K_2 using linear least squares. The process is iterated until converged.

IV. RESULTS AND DISCUSSION

To clarify two other artifacts which depend on $|\mathbf{q}|$, we fitted effective constants “ $K_1(n)$ ” and “ $K_2(n)$ ” separately for each shell n defined by $|\mathbf{q}|^2 = n(2\pi/L)^2$; the results are shown in Fig. 1, for selected temperatures. The continuum approximation must break down at the CCT linkage length scale ($\sim 2.5a_R$), which explains the deviations visible for $n \geq 20$, i.e. $2\pi/|\mathbf{q}| \leq 4.2a_R$. (Above the supertile formation temperature, the tile length scale is the rhombohedron edge a_R , and no such deviations are seen in this wavevector range.)

At small wavevectors, equilibration time becomes problematic. As shown in Ref. 22, eqs. (20ff), the relaxation rates of $\tilde{\mathbf{h}}(\mathbf{q})$ are $\gamma C_i(\mathbf{q})$, where $\gamma(T)$ is a relaxation coefficient and $\{C_1, C_2, C_3\}$ are the eigenvalues of $\mathbf{C}(\mathbf{q})$. This becomes problematic when temperature is low (since $\gamma(T) \rightarrow 0$ as $T \rightarrow 0$) and $|\mathbf{q}|$ is small (as $\mathbf{C} \propto |\mathbf{q}|^2$, eq. (5)). The consequence is that, at the lowest temperatures in Fig. 1, the smallest wavevectors are governed by the elastic constants of the higher temperature at which these modes fell out of equilibrium.

The plots in Fig. 1 suggest two regimes as a function of wavevector and temperature.²⁴ At high T or large

wavevector, a linear dependence on $n \propto |\mathbf{q}|^2$ is visible, with the slope increasing as $T \rightarrow 0$. We attribute this to our use of the 3DPT vertices in (9): the \mathbf{x}^\perp differences between adjacent vertices (separated by a_R) certainly exceed the fluctuations of the smooth $\mathbf{h}(\mathbf{r})$ surface, extrapolated to this short scale. Consequently, the inferred elastic constant is spuriously small.

On the other hand, a second regime is visible at low T and $|\mathbf{q}| < \kappa(T)$, where $\kappa(T)$ defines a crossover. In this regime, $K_i(n)$ has a clear linear dependence, which we tentatively attribute to higher-order-gradient terms of $O(q^4)$ in the harmonic phason-elastic coefficients (5), which are permitted by symmetry. Although it certainly affects the $n = 1, 2$ wavevector shells at the lowest temperatures, lack of equilibration cannot explain all of the low T /small $|\mathbf{q}|$ regime, as the data (in this regime) agree very well with our lattice-gas simulations¹⁵ which have a different dynamics. We used the empirical fitting form

$$K_i(n) = a_i + b_i \sqrt{n^2 + n_\kappa^2} + c_i \frac{n}{\sqrt{n^2 + n_\kappa^2}} \quad (12)$$

to extrapolate $K_1(n)$ and $K_2(n)$ to $\mathbf{q} = 0$.

Our principal result is the temperature dependence of the elastic constants indicated on Fig. 2. At infinite temperature, i.e. for the maximally random tiling, we fit $K_1 = 0.84$ and $K_2 = 0.52$, so $K_2/K_1 = 0.62$ in agreement with previous measurements on the same ensemble^{21,22}. As temperature decreases, K_1 increases, as expected since the Hamiltonian (1) favors formation of “supertiles” which have small perp-space differences among their corner nodes. Meanwhile, K_2/K_1 turns negative with decreasing temperature, consistent with our knowledge that the random CCT²⁵ has $K_2 < 0$. It appears that $K_1 \rightarrow 2.26$ and $K_2 \rightarrow -1.44$ as $T \rightarrow 0$, thus $K_2/K_1 \rightarrow -0.64$, with errors of order 10%. Our lattice-gas simulations¹⁵ gave similar results.

Approaching $T = 0$, the fit of our data to the angular dependence of elastic theory may be worsening. Furthermore, K_2/K_1 seems to be approaching the critical value -0.75 , at which the system goes unstable to a modulation with \mathbf{q} and $\tilde{\mathbf{h}}(\mathbf{q})$ along a 3-fold axis. This suggests that the true canonical-cell tiling – more precisely the maximum-density subensemble of the CCT – might have a more complicated dependence than elastic theory. This is not unprecedented: exactly that is known to happen in those 10-fold and 12-fold symmetric two-dimensional tilings¹³ that have extra constraints like the CCT.

Neutron and X-ray diffraction measurements of diffuse wings around Bragg peaks yield $K_2/K_1 = -0.5$ for *i*-AlPdMn^{9,10,11}, agreeing with our result, so *i*-AlPdMn might be modeled by a CCT-like network of microscopic clusters. On the other hand, *i*-AlCuFe has $K_2/K_1 > 0$ ¹¹. Thus, despite their similar face-centered icosahedral atomic structures, *i*-AlPdMn and *i*-AlCuFe must be modeled by different tile Hamiltonians.

The recent experimental calibration of *i*-AlPdMn data¹⁰ yielded $K_1/T = 0.002\text{\AA}^{-3}$ in absolute physical units. Multiplying by a_R^3 (with $a_R = 4.5\text{\AA}$) converts this

to $K_1 \approx 0.2$ in the units of this paper, which is puzzlingly small. This is hard to explain by a misjudgment in our model formulation. If our tiles are invalid, one expects that (since this alloy is so well ordered), they should be replaced by large supertiles, so that K_1 becomes *larger*, or that matching rules are satisfied implying $K_1 \rightarrow \infty$. Instead, the data suggest that, implausibly, atoms are free to fluctuate in groups even *smaller* than a rhombohedron.

The temperature dependence of $K_i(T)$ was used for extrapolation only; the Hamiltonian (1) simply implements the CCT and is unlikely to model a realistic quasicrystal. A physically relevant model would add to (1) an additional perturbation α' that breaks the degeneracy among canonical-cell tilings, so that large α' corresponds to physical low temperature. Such a model can be investigated using the techniques of this paper.

In conclusion, we evaluated the phason elastic constants of the canonical-cell tiling for the first time, by a simulation in which the mean-square fluctuations of the abstract surface representing the tile configuration were measured at many wavevectors. This is the first theoretical measurement in any quasicrystal model of the temperature dependence of the phason elastic constants.

Acknowledgments

This work is supported by DOE grant DE-FG02-89ER45405; computer facilities were provided by the Cornell Center for Materials Research under NSF grant DMR-9632275. We thank M. de Boissieu for discussions.

-
- * Materials Research and Liquids, Institute of Physics, TU Chemnitz, D-09107 Chemnitz, Germany; Current and permanent address, Institute of Physics, Slovak Academy of Sciences, 84228 Bratislava, Slovakia.
- ¹ See e.g. S. W. Kycia *et al*, Phys. Rev. B 48, 3544 (1993).
 - ² C. L. Henley, "Random tiling models," p. 429 in *Quasicrystals: The State of the Art*, ed. P. J. Steinhardt and D. P. DiVincenzo, (World Scientific, 1991).
 - ³ C. L. Henley, Phys. Rev. B **43**, 993 (1991).
 - ⁴ M. Windisch, J. Hafner, M. Krajčí and M. Mihalkovič, Phys. Rev. B 49, 8701 (1994).
 - ⁵ M. Mihalkovič *et al*, Phys. Rev. B 53, 9002 (1996).
 - ⁶ K. Ingersent in *Quasicrystals: The State of the Art*, eds. D. P. DiVincenzo and P. J. Steinhardt (World Scientific, 1991).
 - ⁷ H.-C. Jeong and P.J. Steinhardt, Phys. Rev. Lett. 73, 1943 (1994).
 - ⁸ M. Widom, Phil. Mag. Lett. 64, 297 (1991); Y. Ishii, Phys. Rev. B 45, 5228 (1992).
 - ⁹ M. de Boissieu, *et al*, Phys. Rev. Lett. 75, 89 (1995).
 - ¹⁰ A. Létoublon *et al*, Phil. Mag. Lett. 81, 273 (2001).
 - ¹¹ A. Létoublon, thesis (Grenoble, France), 1998.
 - ¹² M. Mihalkovič and P. Mrafko, Europhys. Lett. 21, 463 (1993).
 - ¹³ M. Oxborrow and C. L. Henley, Phys. Rev. B 48, 6966 (1993); M. Oxborrow and M. Mihalkovič, p. 451 in *Aperiodic '97*, eds. M. de Boissieu, J.-L. Verger-Gaugry, and R. Currat (World Scientific, 1998).
 - ¹⁴ H.-C. Jeong and P.J. Steinhardt Phys. Rev. B 48, 9394 (1993); T. Dotera and P. J. Steinhardt, Phys. Rev. Lett. 72, 1670 (1994).
 - ¹⁵ M. Mihalkovič and C. L. Henley, in preparation.
 - ¹⁶ C. L. Henley, Phys. Rev. B 34, 797 (1986).
 - ¹⁷ M. V. Jarić and D. R. Nelson, Phys. Rev. B 37, 4458 (1988).
 - ¹⁸ V. Elser, Phys. Rev. B **32**, 4892 (1985).
 - ¹⁹ T. C. Lubensky, in *Aperiodic Crystals I: Introduction to Quasicrystals*, M. V. Jarić (ed.), (Academic Press, London, 1988), and references therein.
 - ²⁰ W. Li, *et al*, J. Stat. Phys. **66**, 1 (1992), and references therein.
 - ²¹ L.-H. Tang, Phys. Rev. Lett. **64**, 2390 (1990).
 - ²² L. J. Shaw, V. Elser, and C. L. Henley, Phys. Rev. B 43, 3423 (1991).
 - ²³ C. L. Henley, V. Elser, and M. Mihalkovič, Z. Kristallogr 215, 553 (2000).
 - ²⁴ We do not know the origin of the anomalies in the range $12 \leq n \leq 20$ (the irregularities in Fig. 1 are not statistical, except perhaps in the small- $|\mathbf{q}|$ /low- T limit.)
 - ²⁵ M. E. J. Newman and C. L. Henley, Phys. Rev. B 52, 6386 (1995).

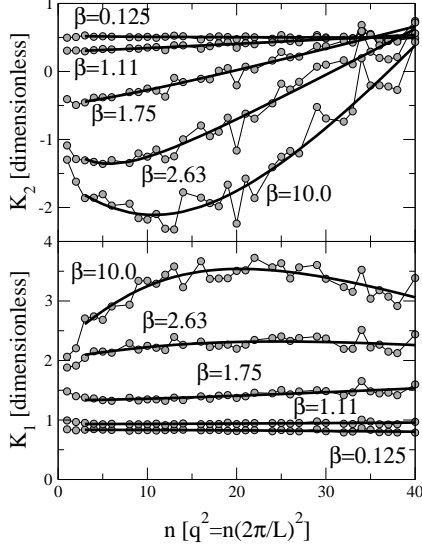


FIG. 1: Phason elastic constants K_1 (bottom) and K_2/K_1 (top), where K_1 and K_2 are fitted from “perp” space fluctuation $\Gamma^{H_{lm}}(\mathbf{q})$ of rhombohedron vertices, Fourier-transformed and separately fitted in each shell of wavevector $\mathbf{q} = \sqrt{n}(2\pi/L)$. Bragg peaks and tails were subtracted using (10). Only five of the 34 temperatures are shown (labeled by $\beta \equiv 1/T$). The fits to Eq. (12) are shown as solid lines.

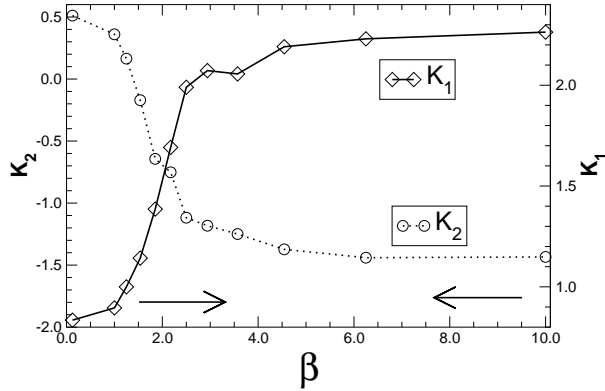


FIG. 2: Elastic constants as a function of inverse temperature β . These are same fitted values indicated by solid lines in Fig. 1, extracted from the perp-coordinates of rhombohedron vertices and extrapolated to $q \rightarrow 0$.